

Morphometric analysis of vidian canal and its relations with surrounding anatomic structures by using cone-beam computed tomography

M.H. Kurt¹, P. Bozkurt², B. Bilecenoğlu³, M.E. Kolsuz¹, K. Orhan¹

¹Department of Dentomaxillofacial Radiology, Faculty of Dentistry, Ankara University, Ankara, Turkey

²Department of Oral and Maxillofacial Surgery, Faculty of Dentistry, Ankara University, Ankara, Turkey

³Department of Basic Sciences, Anatomy Division, Faculty of Dentistry, Ankara University, Ankara, Turkey

[Received: 24 May 2019; Accepted: 5 August 2019]

Background: We identified the vidian canal (VC) in a Turkish subpopulation on cone-beam computed tomography (CBCT) images and explored its anatomic relationships; the canal serves as an anatomic pathway during endonasal surgical approaches.

Materials and methods: Coronal and axial CBCT images of 100 patients (50 males and 50 females) were evaluated (slice thickness and interval, 0.5 mm). We measured the length of the VC length, extent of VC pneumatization into the sphenoid sinus, position of the VC relative to the medial pterygopalatine plate (MPP), pterygopalatine fossa (PPF) depth, and VC-VC, VC-MPP, and VC-foramen rotundum (FR) distances, the angle between the posterior end of the middle turbinate and the lateral part of the VC anterior opening, and the angle between the VC and the palatovaginal canal.

Results: The mean VC length was 13.09 ± 2.07 and 13.01 ± 2.12 mm on the right and left sides, respectively. Relative to the MPP, the VC was located medially in 54.5% of patients, on the same level in 36%, and laterally in 9.5%. Pneumatization was of grade I in 24% of patients, grade II in 33%, grade III in 23.5%, and grade IV in 19.5%. The VC-FR and VC-MPP distances were significantly greater on the left side. The angle between the posterior end of the middle turbinate and the lateral part of the anterior VC opening was significantly greater on the right side. The VC-VC distance was significantly greater when the VC lay lateral to the MPP.

Conclusions: Anatomic characteristics of the VC on CBCT images unique to Turkish populations should be kept in mind during surgery. (Folia Morphol 2020; 79, 2: 366–373)

Key words: endonasal approach, vidian canal, cone-beam computed tomography, morphometric analysis, pterygoid canal, vidian nerve

INTRODUCTION

A surgical endoscopic endonasal approach (EEA) is used to treat selected skull base lesions [16, 24, 25, 44] and to control the symptoms of vasomotor rhinitis (clear rhinorrhoea and nasal congestion) via vidian neurectomy, as described by Golding-Wood [17].

EEA techniques are less invasive, and more rapid and direct, than conventional transantral and transpalatal techniques [29, 30, 37]. The vidian canal (VC) is a critical landmark for safe identification of the petrous internal carotid artery. The vidian nerve guides the surgeon to the lateral margin of the anterior genu

of the petrous internal carotid artery, at the level of the foramen lacerum [14, 26, 51]. Professor Vidius (working in the 16th century) described and named several anatomic structures including the vidian nerve, artery, and canal [50]. The VC runs anteriorly from the anterior border of the foramen lacerum, through the sphenoid sinus floor, to end in the pterygopalatine fossa (PPF). Nerves and vessels pass through the VC. The vidian nerve is formed by the greater superficial petrosal nerve (the branch of the facial nerve that contains parasympathetic fibres) and the deep petrosal nerve from the carotid plexus, which contains sympathetic fibres [45]. The nerve passes through the VC to synapse in the sphenopalatine (Meckel's) ganglion. Postganglionic branches are distributed via branches of the maxillary nerve to the lacrimal gland, and the nasal and palatal mucosae [50]. The nerve transmits impulses to the nasal and palatine nerves [45].

Imaging plays a central role in the management of skull base diseases because clinical assessment of this region is often difficult or incomplete. Computed tomography (CT) is ideal for delineation of the bony anatomy and is often combined with magnetic resonance imaging [12]. It is essential to evaluate the relationship between the VC and surrounding structures of the sphenoid sinus via preoperative CT [55]. In the time since the introduction of cone-beam computed tomography (CBCT) for dentomaxillofacial imaging, several novel systems differing in terms of technical specifications and settings have become commercially available. CBCT is now commonly used before or during dental implantology, dentomaxillofacial surgery, image-guided surgical procedures, and orthodontic, periodontic, and endodontic procedures [27, 38]. Compared to CT systems, dental CBCT units are associated with less radiation, lower costs, shorter scan times, simpler imaging protocols using isotropic voxels, and high spatial resolution [18, 35, 46].

Here, we studied important anatomical landmarks of the VC on CBCT images. To the best of our knowledge, preoperative mapping of the VC using CBCT has not been extensively explored. Operators can examine the surgical area to plan an ideal approach.

MATERIALS AND METHODS

CBCT images

This retrospective study was based on CBCT images of 200 VCs of 100 patients (50 males and 50 females) referred to our outpatient clinic in Ankara, Turkey. CBCT images were obtained using a Planmeca Promax

3D Max (Planmeca Oy, Helsinki, Finland; field-of-view, 230 × 160 mm). The raw data were reconstructed at an isotropic voxel size of 0.40 mm³ and a slice thickness and interval of 0.5 mm. Low-quality images that did not show bone borders clearly, those with artefacts, and those of insufficient magnification were excluded.

CBCT evaluation

All evaluations were performed using inbuilt software (Romexis ver. 3.7; Planmeca Oy, Helsinki, Finland) and a 21.3-inch flat-panel colour-active matrix TFT medical display (MultiSync MD215MG; NEC, Munich, Germany) with a resolution of 2,048 × 2,560 pixels at 75 Hz, and a 0.17-mm dot pitch operating at 11.9 bits. Images were reconstructed and observed in the sagittal, axial, and coronal planes. All measurements were made in a dimly lit room by a maxillofacial radiologist with 11 years of experience (MHK). The radiologist adjusted image brightness and contrast according to personal preference. Morphometric measurements were made on coronal and axial sections. On coronal sections, the VC-VC, VC-medial pterygopalatine plate (MPP), and VC-foramen rotundum (FR) distances were measured (Fig. 1). The pneumatization pattern of the VC (into the sphenoid sinus) was evaluated according to Vescan et al. [51] (grade I: completely surrounded by bone; grade II: VC surrounded by air for 33% of the circumference; grade III: VC surrounded by air for 33–66% of the circumference; grade IV: VC almost completely surrounded by air) (Fig. 2). The VC position relative to the MPP was recorded as either medial, on the same line, or lateral (Fig. 3). The VC length, PPF depth, the angle between the posterior end of the middle turbinate and the lateral part of the VC anterior opening, and the angle between the palatosphenoidal canal and the VC, were measured on axial sections (Fig. 4).

Statistical analysis

All statistical analyses were performed using IBM SPSS software (ver. 20.0; SPSS Inc., Chicago, IL, USA). Descriptive statistics are presented as means ± standard deviations. The paired t-test was used to explore whether differences between sides and genders were significant ($p \leq 0.05$). A one-way ANOVA test was used to compare continuous variables; the confidence level was set to 95%. The *post-hoc* Tukey test was used to compare the groups when the ANOVA data were statistically significant. A p -value < 0.05 was considered to reflect statistical significance. The Bonferroni adjustment was applied to control for type I error in all multiple comparisons.

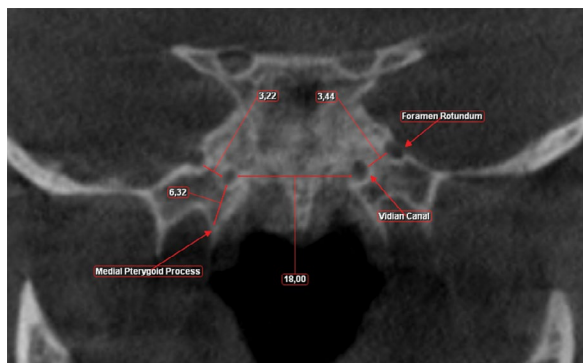


Figure 1. Distances between vidian canal and surrounding structures on coronal plane.

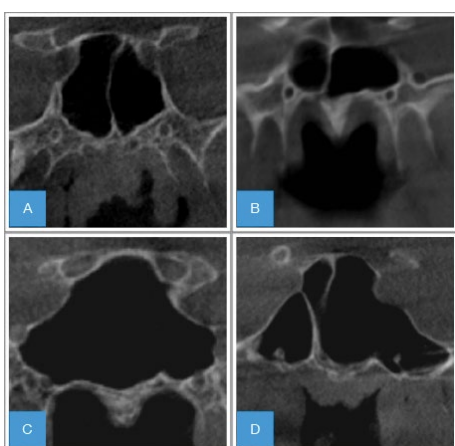


Figure 2. The pneumatization degree of vidian canal into the sphenoid sinus according to the Vescan et al. [51]; **A.** Grade I: completely surrounded by bone; **B.** Grade II: a canal surrounded by air for 1/3 of its circumference; **C.** Grade III: a canal surrounded by air for 1/3 to 2/3 of its circumference; **D.** Grade IV: almost entirely surrounded by air.

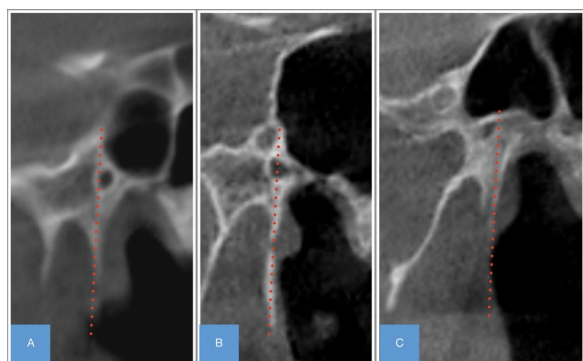


Figure 3. The position of the vidian canal relative to medial pterygopalatine plate on coronal plane; **A.** Medial; **B.** Straight; **C.** Lateral.

RESULTS

We reviewed images of 200 VCs from 50 females and 50 males with a mean age of 48.53 ± 19.25 and

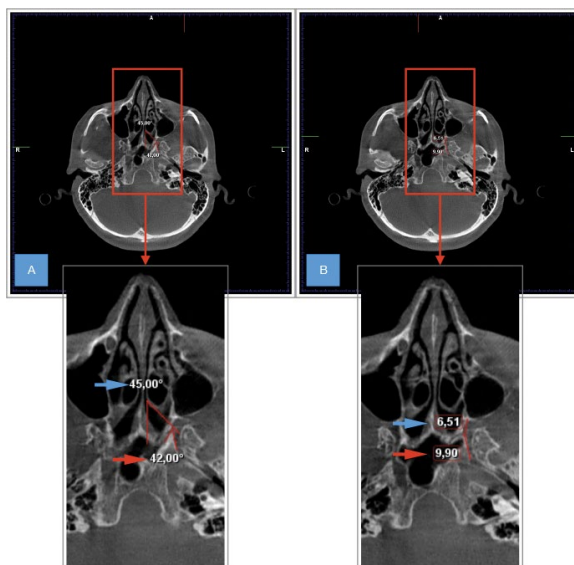


Figure 4. A. The angle between the posterior end of the middle turbinate and the anterior opening of the vidian canal (VC) (blue arrow); the angle between palatovaginal canal and VC (red arrow); **B.** Measurement of the length of VC (red arrow) and the depth of pterygopalatine fossa (blue arrow).

43.46 ± 18.67 years, respectively. The VC pneumatization grades (into the sphenoid sinus) followed Vescan et al. [51]. Overall, 24% of the patients were grade I, 33% were grade II, 23.5% were grade III, and 19.5% were grade IV. The VC was located medial to the MPP in 54.5% of images ($n = 109$), on the same level as the MPP in 36% ($n = 72$), and lateral to the MPP in 9.5% (Fig. 2). Neither the proportion of pneumatization nor the VC location relative to the MPP differed significantly by side or gender (both $p > 0.05$).

The mean VC length was 13.09 ± 2.07 mm on the right side and 13.01 ± 2.12 mm on the left side. The angle between the posterior end of the middle turbinate and the lateral part of the VC anterior opening was significantly greater on the right; the VC-FR and VC-MPP distances were significantly greater on the left side (all $p \leq 0.05$). The other measurements did not differ significantly by side (Table 1). All values were somewhat higher in males, except the angle between the posterior end of the middle turbinate and the lateral part of the VC anterior opening, but the differences were not statistically significant (Table 2).

The right PPF depth was significantly lower, and the VC-VC and VC-FR distances were significantly greater, when the VC lay lateral to the MPP (all $p \leq 0.05$). The angle between the posterior end of the middle turbinate and the lateral part of the VC anterior opening, and the VC-MPP distance, were

Table 1. Descriptive statistics and the results of the measurements for right and left sides; p-values belong to paired t-test ($p \leq 0.05$)

Parameters	Left	Right	P
VC-VC	24.17 ± 2.84		
VC-MPP	8.28 ± 2.77	7.86 ± 2.80	0.04*
VC-FR	4.75 ± 2.26	4.39 ± 2.22	0.03*
Length of vidian canal	13.01 ± 2.12	13.09 ± 2.07	> 0.05
Pterygopalatine fossa depth	9.29 ± 1.81	9.32 ± 1.96	> 0.05
Angle between palatosphenoid canal and vidian canal	66.12 ± 14.74	65.87 ± 14.30	> 0.05
Angle between posterior end of middle turbinate and lateral part of the vidian canal anterior opening	32.07 ± 8.2	34.94 ± 9.93	0.02*

*Significant difference; VC-VC — vidian canal-vidian canal; VC-MPP — vidian canal-medial pterygopalatine plate; VC-FR — vidian canal-foramen rotundum

Table 2. The mean values for the parameters measured for each gender; p-values belong to paired t-test ($p \leq 0.05$)

Parameters	Females	Males	P
VC-VC (coronal plane)	23.56 ± 2.83	24.93 ± 2.80	> 0.05
Length of the vidian canal (axial plane)	12.80 ± 1.96	13.29 ± 2.17	> 0.05
Depth of pterygopalatine fossa (axial plane)	8.93 ± 1.87	9.67 ± 1.80	> 0.05
VC-FR (coronal plane)	4.24 ± 1.99	4.89 ± 2.41	> 0.05
VC-MPP (coronal plane)	7.85 ± 2.34	8.27 ± 3.13	> 0.05
Angle between the posterior end of the middle turbinate and lateral part of the vidian canal anterior opening (axial plane)	34.21 ± 9.33	32.82 ± 9.04	> 0.05
Angle between palatosphenoid canal and vidian canal (axial plane)	64.63 ± 14.15	67.43 ± 14.68	> 0.05

VC-VC — vidian canal-vidian canal; VC-FR — vidian canal-foramen rotundum; VC-MPP — vidian canal-medial pterygopalatine plate

significantly greater on the left side when the VC lay lateral to the MPP (both $p \leq 0.05$) (Table 3).

On both sides, the VC-VC distance was longer in images exhibiting grade IV versus grade I pneumatization; the VC-FR distance was longer in images exhibiting grade III or IV pneumatization versus grade I pneumatization, and in images exhibiting grade IV versus grade II pneumatization (all $p \leq 0.05$) (Table 4).

DISCUSSION

The VC is a very important anatomical landmark in the EEA to treat skull base lesions and vasomotor rhinitis [16, 44, 24, 25]. In recent years, the EEA to the VC has been divided into two main types: intrasphenoidal (type I) and transnasal (type II) [20, 34]. The type I approach is associated with a shorter operating time and less bleeding, and is appropriate when the VC-VC and VC-FR distances are long and the lateral distance between the VC and the MPP is not large [48, 55]. The success rate of the type II approach increases significantly as the angle between the posterior end of the middle turbinate and the lateral margin of the anterior opening of the VC decreases [33, 34, 48, 55]. Given the increasing popularity of accessing the VC via the EEA, it is important to determine the relationships of the VC with other neurovascular structures; several radiological/anatomic studies have emphasized the importance of CT in terms of planning [1, 5, 13, 21, 28, 36, 41, 47, 51, 53]. In the present retrospective study, we used CBCT images to measure the VC and explore its relationships with surrounding anatomic structures. Dental CBCT units deliver low radiation doses; furthermore, the scan time is short, imaging is straightforward and the cost is low. We used isotropic voxels to identify VC configurations in the present study [18, 35, 46]. Kassam et al. [25] emphasized that the VC-FR distance was important for the EEA. The mean VC-FR distance ranged from 4 to 8.5 mm in previous studies [6, 8, 19, 24, 55]. In the present study, we found no significant gender difference in the mean VC-FR distance; among the entire cohort, the mean distance was 4.75 ± 2.26 and 4.39 ± 2.22 mm on the left and right sides, respectively.

Mato et al. [36] emphasized that the length of the VC is an important determinant of the extent of bone drilling during surgery. In that study, the average VC length was 14.4 and 14.7 mm on the right and left sides, respectively. Other studies reported VC lengths of 10 to 19 mm [2, 6, 10, 11, 15, 22, 36, 41, 49, 51, 52]. In the present study, the mean VC length was 13.09 ± 2.07 and 13.01 ± 2.12 mm on the right and left sides, respectively, with no significant difference between the genders.

During EEA, it is necessary to open the PPF to reach the anterior opening of the VC. We found that the mean PPF depth was 9.32 ± 1.96 and 9.29 ± 1.81 mm on the right and left sides, respectively, with no significant gender difference. The PPF depth ranged from 6.7 to 7.1 mm on both sides in previous studies [36, 51]. The PPF depth was greater

Table 3. Multiple comparison of the measured parameters of the VC's position relative to MPP; p-values belong to one-way ANOVA test ($p < 0.05$)

Morphometric measurements	Position of VC relative to MPP		Position of VC relative to MPP		
			Medial	Straight	Lateral
Angle between the posterior end of the middle turbinate and the lateral part of the VC anterior openings (coronal plane)	Right	Medial	32.92 ± 10.91	0.088	1.00
		Straight	0.088	37.58 ± 7.46	1.00
		Lateral	1.00	1.00	35.54 ± 11.05
	Left	Medial	30.26 ± 7.38	0.040*	0.745
		Straight	0.040*	34.63 ± 8.74	1.00
		Lateral	0.745	1.00	33.81 ± 9.99
VC-MPP (coronal plane)	Right	Medial	7.92 ± 3.00	1.00	1.00
		Straight	1.00	7.85 ± 2.61	1.00
		Lateral	1.00	1.00	7.57 ± 2.69
	Left	Medial	8.90 ± 2.56	0.32*	1.00
		Straight	0.32*	7.39 ± 2.87	0.638
		Lateral	0.638	1.00	7.67 ± 2.87
PPF depth (axial plane)	Right	Medial	9.56 ± 1.75	1.00	0.029*
		Straight	1.00	9.42 ± 2.25	0.064*
		Lateral	0.029*	0.064*	7.88 ± 1.20
	Left	Medial	9.52 ± 1.87	0.995	0.203
		Straight	0.995	9.15 ± 1.58	0.649
		Lateral	0.203	0.649	8.27 ± 2.07
VC-FR (coronal plane)	Right	Medial	4.28 ± 2.18	1.00	0.004*
		Straight	1.00	3.90 ± 1.74	0.001*
		Lateral	0.004*	0.001*	6.57 ± 2.73
	Left	Medial	4.97 ± 2.24	0.838	1.00
		Straight	0.838	4.43 ± 2.01	1.00
		Lateral	1.00	1.00	4.63 ± 3.42
VC-VC (coronal plane)	Right	Medial	23.55 ± 2.71	0.599	0.002*
		Straight	0.599	24.31 ± 2.73	0.038*
		Lateral	0.002*	0.038*	26.68 ± 2.63
	Left	Medial	23.97 ± 3.02	1.00	1.00
		Straight	1.00	24.53 ± 2.67	1.00
		Lateral	1.00	1.00	24.10 ± 2.42

*Significant differences; VC — vidian canal; MPP — medial pterygopalatine plate; VC-MPP — vidian canal-medial pterygopalatine plate; PPF — pterygopalatine fossa; VC-FR — vidian canal-foramen rotundum; VC-VC — vidian canal-vidian canal

in our study, reflecting differences among Japanese, other Caucasian and Turkish populations.

During EEA, an unusually pronounced or hypertrophic turbinate may compromise operative success. Therefore, it is important to measure the angle between the posterior end of the middle turbinate and the anterior opening of the VC during surgical planning; Liu and Su [33] measured this angle on coronal CT images, as 30.2 ± 4.9 and $26.4 \pm 9.1^\circ$ in those for whom operations were successful and 33.8 ± 4.8 and $44.3 \pm 8.1^\circ$ in those for whom operations failed on the right

and left sides, respectively. Açar et al. [2] reported an angle of $33.05 \pm 7.71^\circ$ in a Turkish subpopulation; we measured mean angles of 34.94 ± 9.93 and $32.07 \pm 8.2^\circ$ on the right and left sides, respectively; the angle on the right was significantly greater ($p \leq 0.05$) and there was no significant gender difference in the angles.

The palatovaginal canal is also a key anatomic landmark for intraoperative identification of the VC; a good knowledge of radiologic anatomy is essential to avoid misidentification of the palatovaginal canal as the VC [23, 43]. Several studies have measured

Table 4. Multiple comparison of the measured distance (VC-FR and VC-VC) according to pneumatisation grades; p-values belong to one-way ANOVA test ($p < 0.05$)

Morphometric measurements		Pneumatisation degree				
		Grade I	Grade II	Grade III	Grade IV	
VC-VC (coronal plane)	Right	Grade I	23.13 ± 2.48	1.00	0.454	0.44*
		Grade II	1.00	24.10 ± 2.79	1.00	0.593
		Grade III	0.454	1.00	24.54 ± 3.13	1.00
		Grade IV	0.44*	0.593	1.00	25.49 ± 2.68
	Left	Grade I	22.82 ± 2.34	0.553	0.788	0.006*
		Grade II	0.553	24.07 ± 2.71	1.000	0.256
		Grade III	0.788	1.000	24.07 ± 2.71	0.301
		Grade IV	0.006*	0.256	0.301	24.07 ± 2.71
VC-FR (coronal plane)	Right	Grade I	3.04 ± 1.39	0.298	0.001*	0.000*
		Grade II	0.298	4.06 ± 2.15	0.228	0.004*
		Grade III	0.001*	0.228	5.18 ± 1.97	0.877
		Grade IV	0.000*	0.004*	0.877	6.11 ± 2.33
	Left	Grade I	3.17 ± 1.25	0.190	0.002*	0.000*
		Grade II	0.190	4.42 $\pm 2.25^*$	395	0.037*
		Grade III	0.002*	395	5.45 ± 2.20	1.000
		Grade IV	0.000*	0.037	1.000	6.01 ± 2.18

*Significant differences; VC-VC — vidian canal-vidian canal; VC-FR — vidian canal-foramen rotundum

the distance between the VC and the palatovaginal canal, although to the best of our knowledge, only one measured the angle ($48 \pm 12.28^\circ$) [6, 43, 53, 55]. In this study, the angles were 66.12 ± 14.74 and $65.87 \pm 14.30^\circ$ on the left and right sides, respectively, and did not differ by gender.

During EEA, the MPP usually needs to be drilled, so it is essential to determine the location of the VC relative to the MPP when planning surgery [51]. Yeh and Wu [55] evaluated the position of the VC relative to the MPP; in 98.1% of cases the VC was positioned medially

or lay on the same line, and in 1.9% of cases it was positioned laterally. Mato et al. [36] found that, on the right side, the VC lay medial to the MPP in 90.9% of cases, while in 8.7% of cases it was on the same line, and in 0.4% of cases it lay lateral to the MPP; the respective values on the left side were 86.1%, 12.1%, and 1.7%. Our results are similar to those of previous studies except that the VC lay medial to the MPP in a higher proportion of cases. Yazar et al. [53] and Bahşi et al. [5] found that the VC often lay on the same line as the MPP in Turkish populations; differences in VC location among studies may reflect differences in population sizes and racial characteristics.

In this study, the PPF depth on the right was lower, and the VC-FR and VC-VC distances were significantly greater, when the VC lay lateral to the MPP ($p \leq 0.05$). The angle between the posterior end of the middle turbinate and the lateral VC anterior opening, and the VC-MPP distance, were significantly greater on the left side when the VC lay lateral to the MPP ($p \leq 0.05$). The VC-FR distance was 4.75 ± 2.26 mm on the left side and 4.39 ± 2.22 mm on the right side; the distance was significantly greater on the left side ($p \leq 0.05$).

The extent of pneumatisation is important during EEA. If pneumatisation is marked, less bone drilling is required. In addition, foreknowledge of the extent of pneumatisation reduces the likelihood of surgical injury to surrounding anatomical structures, such as the FR or anterior genu of the internal carotid artery [14, 49]. The extent of VC pneumatisation into the sphenoid sinus varies by VC type, as described in the literature. Yeh and Wu [55] categorised the VC as follows: type 1, within the sphenoid corpus; type 2, partially protruding into the sphenoid sinus; and type 3, stalked and protruding completely into the sphenoid sinus. Vescan et al. [51] developed the following system for grading pneumatisation by VC circumference: grade I, entirely surrounded by bone; grade II, surrounded by air over 33% of the circumference; grade III, surrounded by air over 33–66% of the circumference; and grade IV, almost completely surrounded by air. We used this classification system because it is more detailed and simpler than other systems.

Although some authors [2, 5, 32, 52, 55] consider that a VC located near the pterygoid process and the fused sphenoid bone as type 1, others classified such cases as type 3 [3, 31, 39, 42, 54]. Chen and Xiao [10] classified the VC as A, B, or C. Bidarkotimath et al. [6], Omami et al. [40], and Yazar et al. [53] classified VC by location but not type. In our study, grade II VCs were

the most common (33%), and grade IV were the least common (19.5%). Grades IV and I were least common on the right and left sides, respectively, in line with the results of other studies [36, 51]. Açar et al. [2] reported type 1 VC in 55.6% of cases, type 2 in 34.8%, and type 3 in 9.6%. Bidarkotimath et al. [6], Yeh et al. [55], Chen and Xiao, [10] and Cankal et al. [9] reported type 1 VC in 67%, 50.8%, 55%, and 54% of cases, type 2 in 22%, 39.8%, 31%, and 36%, and type 3 in 11%, 9.4%, 14%, and 10%, respectively. Al-Sheibani et al. [4] reported that type 1 and 2 VCs were more remote from surrounding anatomic structures. Bolger [7] emphasized that VC type 3 was associated with a greater risk of damage to adjacent structures. Vescan et al. [51] found that the mean VC-FR distance was greater when grade III or IV pneumatization was evident on either the right or left side. We found that the VC-FR distance was greater in patients with pneumatization grades of III or IV rather than grade I, and was greater on both sides in those with grade IV versus grade II pneumatization ($p \leq 0.05$).

CONCLUSIONS

Although many studies have used CT to evaluate the VC and its anatomic relationships, we employed CBCT because it is associated with a low radiation dose that limits the negative effects of radiation. Randomised controlled studies comparing CT and CBCT images are required. We evaluated important morphometric features that can serve as anatomic landmarks. Our data will assist surgeons in obtaining preoperative measurements, and identifying the VC and its relationships with surrounding landmarks. This should reduce the incidence of neurovascular injuries and increase the success rates of surgical procedures.

REFERENCES

- Abuzayed B, Tanriover N, Gazioglu N, et al. Extended endoscopic endonasal approach to the pterygopalatine fossa: anatomic study. *J Neurosurg Sci*. 2009; 53(2): 37–44, indexed in Pubmed: [19546841](#).
- Açar G, Çiçekcibaş AE, Çukurova İ, et al. The anatomic analysis of the vidian canal and the surrounding structures concerning vidian neurectomy using computed tomography scans. *Braz J Otorhinolaryngol*. 2019; 85(2): 136–143, doi: [10.1016/j.bjorl.2017.11.008](#), indexed in Pubmed: [29337014](#).
- Alam-Eldeen MH, ElTaher M, Fadle KN. CT evaluation of pterygoid process pneumatization and the anatomic variations of related neural structures. *gypt J Radiol Nucl Med*. 2018; 49(3): 658–662, doi: [10.1016/j.ejrm.2018.03.011](#).
- Al-Sheibani S, Zanation AM, Carrau RL, et al. Endoscopic endonasal transpterygoid nasopharyngectomy. *Laryngoscope*. 2011; 121(10): 2081–2089, doi: [10.1002/lary.22165](#), indexed in Pubmed: [21898447](#).
- Bahşi İ, Orhan M, Kervancıoğlu P, et al. The anatomical and radiological evaluation of the Vidian canal on cone-beam computed tomography images. *Eur Arch Otorhinolaryngol*. 2019; 276(5): 1373–1383, doi: [10.1007/s00405-019-05335-6](#), indexed in Pubmed: [30747319](#).
- Bidarkotimath S, Viveka S, Udyavar A. Vidian canal radiological anatomy and functional correlations. *J Morphol Sci*. 2012; 29(1): 27–31.
- Bolger WE. Endoscopic transpterygoid approach to the lateral sphenoid recess: surgical approach and clinical experience. *Otolaryngol Head Neck Surg*. 2005; 133(1): 20–26, doi: [10.1016/j.otohns.2005.03.063](#), indexed in Pubmed: [16025047](#).
- Bryant L, Goodmurphy CW, Han JK. Endoscopic and three-dimensional radiographic imaging of the pterygopalatine and infratemporal fossae: improving surgical landmarks. *Ann Otol Rhinol Laryngol*. 2014; 123(2): 111–116, doi: [10.1177/0003489414523707](#), indexed in Pubmed: [24574466](#).
- Cankal F, Haholu A, Kiliç C, et al. CT evaluation of the vidian canal localization. *Clin Anat*. 2007; 20(7): 751–754, doi: [10.1002/ca.20496](#), indexed in Pubmed: [17471528](#).
- Chen J, Xiao J. Morphological study of the pterygoid canal with high-resolution CT. *Int J Clin Exp Med*. 2015; 8(6): 9484–9490, indexed in Pubmed: [26309612](#).
- Cheng Ye, Gao H, Song Ge, et al. Anatomical study of pterygoid canal (PC) and palatovaginal canal (PVC) in endoscopic trans-sphenoidal approach. *Surg Radiol Anat*. 2016; 38(5): 541–549, doi: [10.1007/s00276-015-1597-2](#), indexed in Pubmed: [26691918](#).
- Chong V, Khoo J, Fan YF. Imaging of the nasopharynx and skull base. *Neuroimag Clin N Am*. 2004; 14(4): 695–719, doi: [10.1016/j.nic.2004.07.014](#).
- Erdogan N, Unur E, Baykara M. CT anatomy of pterygopalatine fossa and its communications: a pictorial review. *Comput Med Imaging Graph*. 2003; 27(6): 481–487, doi: [10.1016/S0895-6111\(03\)00038-7](#), indexed in Pubmed: [14575781](#).
- Fortes FSG, Sennes LU, Carrau RL, et al. Endoscopic anatomy of the pterygopalatine fossa and the transpterygoid approach: development of a surgical instruction model. *Laryngoscope*. 2008; 118(1): 44–49, doi: [10.1097/MLG.0b013e318155a492](#), indexed in Pubmed: [17989582](#).
- Fu Z, Chen Y, Jiang W, et al. The anatomical and clinical details of the pterygoid canal: a three-dimensional reconstructive virtual anatomic evaluation based on CT. *Surg Radiol Anat*. 2014; 36(2): 181–188, doi: [10.1007/s00276-013-1161-x](#), indexed in Pubmed: [23824143](#).
- Gardner PA, Kassam AB, Thomas A, et al. Endoscopic endonasal resection of anterior cranial base meningiomas. *Neurosurgery*. 2008; 63(1): 36–52; discussion 52, doi: [10.1227/01.NEU.0000335069.30319.1E](#), indexed in Pubmed: [18728567](#).
- Golding-Wood PH. Observations on petrosal and vidian neurectomy in chronic vasomotor rhinitis. *J Laryngol Otol*. 1961; 75: 232–247, doi: [10.1017/s0022215100057716](#), indexed in Pubmed: [13706533](#).
- Hirsch E, Wolf U, Heinicke F, et al. Dosimetry of the cone beam computed tomography Veraviewepocs 3D compared with the 3D Accuitomo in different fields of view. *Dentomaxillofac Radiol*. 2008; 37(5): 268–273, doi: [10.1259/dmfr/23424132](#), indexed in Pubmed: [18606748](#).
- Hwang SeH, Joo YH, Seo JH, et al. Three-dimensional computed tomography analysis to help define an endoscopic endonasal approach of the pterygopalatine fossa. *Am J Rhinol Allergy*. 2011; 25(5): 346–350, doi: [10.2500/ajra.2011.25.3638](#), indexed in Pubmed: [22186250](#).
- Isaacs SJ, Goyal P. Endoscopic anatomy of the pterygopalatine fossa. *Am J Rhinol*. 2007; 21(5): 644–647, doi: [10.2500/ajr.2007.21.3085](#), indexed in Pubmed: [17999806](#).
- Kamel R, Zaher S. Endoscopic transnasal vidian neurectomy. *Laryngoscope*. 1991; 101(3): 316–319, doi: [10.1288/00005537-199103000-00017](#), indexed in Pubmed: [2000022](#).
- Karci B, Midilli R, Erdogan U, et al. Endoscopic endonasal approach to the vidian nerve and its relation to the sur-

- rounding structures: an anatomic cadaver study. *Eur Arch Otorhinolaryngol.* 2018; 275(10): 2473–2479, doi: [10.1007/s00405-018-5085-2](https://doi.org/10.1007/s00405-018-5085-2), indexed in Pubmed: [30083826](https://pubmed.ncbi.nlm.nih.gov/30083826/).
23. Karligiotis A, Volpi L, Abbate V, et al. Palatovaginal (pharyngeal) artery: clinical implication and surgical experience. *Eur Arch Otorhinolaryngol.* 2014; 271(10): 2839–2843, doi: [10.1007/s00405-014-3111-6](https://doi.org/10.1007/s00405-014-3111-6), indexed in Pubmed: [24902801](https://pubmed.ncbi.nlm.nih.gov/24902801/).
 24. Kasemsiri P, Solares CA, Carrau RL, et al. Endoscopic endonasal transpterygoid approaches: anatomical landmarks for planning the surgical corridor. *Laryngoscope.* 2013; 123(4): 811–815, doi: [10.1002/lary.23697](https://doi.org/10.1002/lary.23697), indexed in Pubmed: [23529878](https://pubmed.ncbi.nlm.nih.gov/23529878/).
 25. Kassam AB, Gardner P, Snyderman C, et al. Expanded endonasal approach: fully endoscopic, completely transnasal approach to the middle third of the clivus, petrous bone, middle cranial fossa, and infratemporal fossa. *Neurosurg Focus.* 2005; 19(1): E6, indexed in Pubmed: [16078820](https://pubmed.ncbi.nlm.nih.gov/16078820/).
 26. Kassam AB, Vescan AD, Carrau RL, et al. Expanded endonasal approach: vidian canal as a landmark to the petrous internal carotid artery. *J Neurosurg.* 2008; 108(1): 177–183, doi: [10.3171/JNS.2008.108.01.0177](https://doi.org/10.3171/JNS.2008.108.01.0177), indexed in Pubmed: [18173330](https://pubmed.ncbi.nlm.nih.gov/18173330/).
 27. Kau CH, Bozic M, English J, et al. Cone-beam computed tomography of the maxillofacial region: an update. *Int J Med Robot.* 2009; 5(4): 366–380, doi: [10.1002/rcs.279](https://doi.org/10.1002/rcs.279), indexed in Pubmed: [19777550](https://pubmed.ncbi.nlm.nih.gov/19777550/).
 28. Kim HS, Kim DI, Chung IH. High-resolution CT of the pterygopalatine fossa and its communications. *Neuroradiology.* 1996; 38 Suppl 1: S120–S126, doi: [10.1007/bf02278138](https://doi.org/10.1007/bf02278138), indexed in Pubmed: [8811698](https://pubmed.ncbi.nlm.nih.gov/8811698/).
 29. Lee JC, Hsu CH, Kao CH, et al. Endoscopic intrasphenoidal vidian neurectomy: how we do it. *Clin Otolaryngol.* 2009; 34(6): 568–571, doi: [10.1111/j.1749-4486.2009.02030.x](https://doi.org/10.1111/j.1749-4486.2009.02030.x), indexed in Pubmed: [20070769](https://pubmed.ncbi.nlm.nih.gov/20070769/).
 30. Lee JC, Kao CH, Hsu CH. Endoscopic vidian neurectomy. An on-line video tutorial: how to do it. *Clin Otolaryngol.* 2010; 35(6): 496–499, doi: [10.1111/j.1749-4486.2010.02206.x](https://doi.org/10.1111/j.1749-4486.2010.02206.x), indexed in Pubmed: [21199414](https://pubmed.ncbi.nlm.nih.gov/21199414/).
 31. Lee JC, Kao CH, Hsu CH, et al. Endoscopic transsphenoidal vidian neurectomy. *Eur Arch Otorhinolaryngol.* 2011; 268(6): 851–856, doi: [10.1007/s00405-010-1482-x](https://doi.org/10.1007/s00405-010-1482-x), indexed in Pubmed: [21221616](https://pubmed.ncbi.nlm.nih.gov/21221616/).
 32. Liu SC, Wang HW, Su WF. Endoscopic vidian neurectomy: the value of preoperative computed tomographic guidance. *Arch Otolaryngol Head Neck Surg.* 2010; 136(6): 595–602, doi: [10.1001/archoto.2010.72](https://doi.org/10.1001/archoto.2010.72), indexed in Pubmed: [20566911](https://pubmed.ncbi.nlm.nih.gov/20566911/).
 33. Liu SC, Su WF. Evaluation of the feasibility of the vidian neurectomy using computed tomography. *Eur Arch Otorhinolaryngol.* 2011; 268(7): 995–998, doi: [10.1007/s00405-011-1497-y](https://doi.org/10.1007/s00405-011-1497-y), indexed in Pubmed: [21290141](https://pubmed.ncbi.nlm.nih.gov/21290141/).
 34. Liu SC, Wang HW, Kao HL, et al. Three-dimensional bone CT reconstruction anatomy of the vidian canal. *Rhinology.* 2013; 51(4): 306–314, doi: [10.4193/Rhin12.189](https://doi.org/10.4193/Rhin12.189), indexed in Pubmed: [24260762](https://pubmed.ncbi.nlm.nih.gov/24260762/).
 35. Ludlow JB, Davies-Ludlow LE, Brooks SL, et al. Dosimetry of 3 CBCT devices for oral and maxillofacial radiology: CB Mercuray, NewTom 3G and i-CAT. *Dentomaxillofac Radiol.* 2006; 35(4): 219–226, doi: [10.1259/dmfr/14340323](https://doi.org/10.1259/dmfr/14340323), indexed in Pubmed: [16798915](https://pubmed.ncbi.nlm.nih.gov/16798915/).
 36. Mato D, Yokota H, Hirono S, et al. The vidian canal: radiological features in Japanese population and clinical implications. *Neurol Med Chir (Tokyo).* 2015; 55(1): 71–76, doi: [10.2176/nmc.0a.2014-0173](https://doi.org/10.2176/nmc.0a.2014-0173), indexed in Pubmed: [25744352](https://pubmed.ncbi.nlm.nih.gov/25744352/).
 37. Minnis NL, Morrison AW. Trans-septal approach for Vidian neurectomy. *J Laryngol Otol.* 1971; 85(3): 255–260, doi: [10.1017/s0022215100073394](https://doi.org/10.1017/s0022215100073394), indexed in Pubmed: [5550607](https://pubmed.ncbi.nlm.nih.gov/5550607/).
 38. Mischkowski RA, Pulsfort R, Ritter L, et al. Geometric accuracy of a newly developed cone-beam device for maxillofacial imaging. *Oral Surg Oral Med Oral Pathol Oral Radiol Endod.* 2007; 104(4): 551–559, doi: [10.1016/j.tripleo.2007.02.021](https://doi.org/10.1016/j.tripleo.2007.02.021), indexed in Pubmed: [17613260](https://pubmed.ncbi.nlm.nih.gov/17613260/).
 39. Mohebbi A, Rajaeih S, Safdarian M, et al. The sphenoid sinus, foramen rotundum and vidian canal: a radiological study of anatomical relationships. *Braz J Otorhinolaryngol.* 2017; 83(4): 381–387, doi: [10.1016/j.bjorl.2016.04.013](https://doi.org/10.1016/j.bjorl.2016.04.013), indexed in Pubmed: [27283380](https://pubmed.ncbi.nlm.nih.gov/27283380/).
 40. Omami G, Hewaidi G, Mathew R. The neglected anatomical and clinical aspects of pterygoid canal: CT scan study. *Surg Radiol Anat.* 2011; 33(8): 697–702, doi: [10.1007/s00276-011-0808-8](https://doi.org/10.1007/s00276-011-0808-8), indexed in Pubmed: [21445687](https://pubmed.ncbi.nlm.nih.gov/21445687/).
 41. Osawa S, Rhoton AL, Seker A, et al. Microsurgical and endoscopic anatomy of the vidian canal. *Neurosurgery.* 2009; 64(5 Suppl 2): 385–411; discussion 411, doi: [10.1227/01.NEU.0000338945.54863.D9](https://doi.org/10.1227/01.NEU.0000338945.54863.D9), indexed in Pubmed: [19404118](https://pubmed.ncbi.nlm.nih.gov/19404118/).
 42. Ozturan O, Yenigun A, Degirmenci N, et al. Co-existence of the Onodi cell with the variation of perisphenoidal structures. *Eur Arch Otorhinolaryngol.* 2013; 270(7): 2057–2063, doi: [10.1007/s00405-012-2325-8](https://doi.org/10.1007/s00405-012-2325-8), indexed in Pubmed: [23274877](https://pubmed.ncbi.nlm.nih.gov/23274877/).
 43. Pinheiro-Neto CD, Fernandez-Miranda JC, Rivera-Serrano CM, et al. Endoscopic anatomy of the palatovaginal canal (palatosphenoid canal): a landmark for dissection of the vidian nerve during endonasal transpterygoid approaches. *Laryngoscope.* 2012; 122(1): 6–12.
 44. Prevedello DM, Pinheiro-Neto CD, Fernandez-Miranda JC, et al. Vidian nerve transposition for endoscopic endonasal middle fossa approaches. *Neurosurgery.* 2010; 67(2 Suppl Operative): 478–484, doi: [10.1227/NEU.0b013e-3181faaa70](https://doi.org/10.1227/NEU.0b013e-3181faaa70), indexed in Pubmed: [21099575](https://pubmed.ncbi.nlm.nih.gov/21099575/).
 45. Rhoton A. The Orbit. *Neurosurgery.* 2002; 51(suppl_4): S1-303-S1-334, doi: [10.1097/00006123-200210001-00008](https://doi.org/10.1097/00006123-200210001-00008).
 46. Scarfe WC, Farman AG, Sukovic P. Clinical applications of cone-beam computed tomography in dental practice. *J Can Dent Assoc.* 2006; 72(1): 75–80, indexed in Pubmed: [16480609](https://pubmed.ncbi.nlm.nih.gov/16480609/).
 47. Solari D, Magro F, Cappabianca P, et al. Anatomical study of the pterygopalatine fossa using an endoscopic endonasal approach: spatial relations and distances between surgical landmarks. *J Neurosurg.* 2007; 106(1): 157–163, doi: [10.3171/jns.2007.106.1.157](https://doi.org/10.3171/jns.2007.106.1.157), indexed in Pubmed: [17236502](https://pubmed.ncbi.nlm.nih.gov/17236502/).
 48. Su WF, Wang HW, Liu SC. Endoscopic vidian neurectomy. The anatomy consideration and preoperative images analysis. *IntechOpen Access.* 2012; 5: 85–105.
 49. Tsutsumi S, Ono H, Ishii H, et al. Visualization of the vidian canal and nerve using magnetic resonance imaging. *Surg Radiol Anat.* 2018; 40(12): 1391–1396, doi: [10.1007/s00276-018-2105-2](https://doi.org/10.1007/s00276-018-2105-2), indexed in Pubmed: [30218150](https://pubmed.ncbi.nlm.nih.gov/30218150/).
 50. Tubbs RS, Salter EG. Vidian vidius (guido guidi): 1509-1569. *Neurosurgery.* 2006; 59(1): 201–3; discussion 201, doi: [10.1227/01.NEU.0000219238.52858.47](https://doi.org/10.1227/01.NEU.0000219238.52858.47), indexed in Pubmed: [16823317](https://pubmed.ncbi.nlm.nih.gov/16823317/).
 51. Vescan A, Snyderman C, Carrau R, et al. Vidian Canal: Analysis and Relationship to the Internal Carotid Artery. *Laryngoscope.* 2007; 117(8): 1338–1342, doi: [10.1097/mlg.0b013e31806146cd](https://doi.org/10.1097/mlg.0b013e31806146cd), indexed in Pubmed: [17572642](https://pubmed.ncbi.nlm.nih.gov/17572642/).
 52. Vuksanovic-Bozarcic A, Vukcevic B, Abramovic M, et al. The pterygopalatine fossa: morphometric CT study with clinical implications. *Surg Radiol Anat.* 2019; 41(2): 161–168, doi: [10.1007/s00276-018-2136-8](https://doi.org/10.1007/s00276-018-2136-8), indexed in Pubmed: [30470877](https://pubmed.ncbi.nlm.nih.gov/30470877/).
 53. Yazar F, Cankal F, Haholu A, et al. CT evaluation of the vidian canal localization. *Clin Anat.* 2007; 20(7): 751–754, doi: [10.1002/ca.20496](https://doi.org/10.1002/ca.20496), indexed in Pubmed: [17471528](https://pubmed.ncbi.nlm.nih.gov/17471528/).
 54. Yeğin Y, Çelik M, Altıntaş A, et al. Vidian Canal Types and Desiccance of the Bony Roof of the Canal: An Anatomical Study. *Turk Arch Otorhinolaryngol.* 2017; 55(1): 22–26, doi: [10.5152/tao.2017.2038](https://doi.org/10.5152/tao.2017.2038), indexed in Pubmed: [29392047](https://pubmed.ncbi.nlm.nih.gov/29392047/).
 55. Yeh IK, Wu IS. Computed tomography evaluation of the sphenoid sinus and the vidian canal. *B-ENT.* 2013; 9(2): 117–121, indexed in Pubmed: [23909118](https://pubmed.ncbi.nlm.nih.gov/23909118/).